AD-A124 259 ACOUSTIC INTENSITY VECTORS INSIDE INFINITE CYLINDRICAL 1/1
ELASTIC SHELL(U) ADMIRALTY MARINE TECHNOLOGY
ESTABLISHMENT TEDDINGTON (ENGLAND.. J H JAMES DEC 82
UNCLASSIFIED AMTE(N)/TM82103 DRIC-BR-86369 F/G 20/1 NL

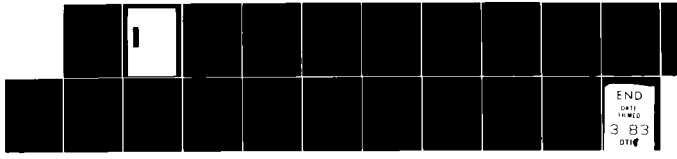

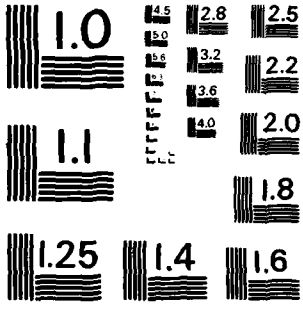

ACOUSTIC INTENSITY VECTORS INSIDE INFINITE CYLINDRICAL ELASTIC SHELL

BY

J H JAMES

Summary

Integral transform formulae are given for the time-harmonic acoustic pressure and particle velocities from which the acoustic intensity vectors in the interior and exterior fluid may be calculated numerically. Some plots of interior intensity vectors due to point-force or point-source excitation demonstrate their potential usefulness as a visual aid to the understanding of wave propagation in fluid-filled pipes.

AMTE (Teddington)
Queen's Road
TEDDINGTON, Middlesex, TW11 0LN

December 1982

26 pages
10 figures

LIST OF SYMBOLS

(x,y,z), (r,ϕ,z)	Cartesian and cylindrical coordinates
$U(\phi,z), V(\phi,z), W(\phi,z)$	axial, tangential and radial displacements at shell mid-surface
α, n	axial and circumferential harmonic wavenumbers
$\overline{U}(n,\alpha), \overline{V}(n,\alpha), \overline{W}(n,\alpha)$	Fourier transforms of shell displacements
$p_1(r,\phi,z)$, $p_2(r,\phi,z)$	interior and exterior pressures
$u_{r1}(r,\phi,z)$, $u_{z1}(r,\phi,z)$	interior acoustic particle displacements
$u_{r2}(r,\phi,z)$, $u_{z2}(r,\phi,z)$	exterior acoustic particle displacements
I	acoustic intensity
w	radian frequency of vibration
ρ_1, c_1	density and sound velocity of interior fluid
ρ_2, c_2	density and sound velocity of exterior fluid
k_i, i=1,2	wavenumber in fluid, w/c_i
a, h, ρ_s	radius, thickness and density of shell
E_1	$=Eh/(1-\sigma^2)$. E is Young's modulus, σ is Poisson's ratio
β^2	$=h^2/12a^2$
e_n	=1 when n=0, and 2 otherwise
F_o	amplitude of point force located at cylindrical coordinates (a,0,0)
p_o	amplitude of point source located at cylindrical coordinates $(x_0,0,0)$
R_o^2	$= (x-x_o)^2+y^2+z^2 = r^2+x_o^2-2rx_o\cos(\phi)+z^2$
$J_n, J_n', Y_n, Y_n', H_n, H_n'$	Bessel functions and their derivatives, $H_n=J_n+iY_n$
b_i, i=1,2	$(k_i^2-\alpha^2)^{\frac{1}{2}}$ with $Im.(b_i)>0$ to satisfy the radiation conditions
η_s, η_f	hyseretic loss factors of shell and fluid
u, p^*	velocity and complex conjugate of pressure

INTRODUCTION

Some recent work by Fuller and Fahy [1] has contributed to the understanding of the physics of wave propagation in piping systems through their discussions on the physical interpretation of the dispersion relation and the energy distribution of free-waves between fluid and shell. James [2,3] has shown that the dispersion relation, presented as wavenumber versus frequency plots, helps to promote a qualitative understanding of sound radiation, power radiation and near-field responses.

Publications by Fahy [4,5] have stimulated interest in the measurement of acoustic intensity using the two-microphone technique. The paper by Reinhart and Crocker [6] provides an instructive account of a practical application. The usefulness of intensity vector plots obtained from theoretical work has been demonstrated by Spicer [7] for the particular case of an elastic plate with mass-spring attachments undergoing forced vibrations. His plots illustrate neatly the physics of the fluid-plate interaction in terms of energy flow in the fluid; in particular, the fluid subsonic surface wave and angled leaky-wave beam are clearly evident.

The main purpose of the work contained herein is to discuss a limited number of wave-frequency and interior acoustic intensity vector plots for the case of an infinite cylindrical elastic shell under the action of point-force or interior point-source excitation. It is hoped that intensity vector plots will display features that enhance the physical interpretation of the wavenumber-frequency plots. The plots may also be of interest to experimenters who are using the technique of acoustic intensity measurement to investigate sound transmission in pipes because a combination of interacting experimental and theoretical work is needed to achieve noise control in complex pipe networks.

2. PROBLEM FORMULATION

(a) General

An infinite cylindrical thin-walled shell contains and is immersed in an acoustic fluid. The displacements of the shell wall satisfy an eighth-order shell theory [8], and the interior and exterior sound pressures satisfy acoustic wave equations. The time-harmonic excitation is provided by mechanical point-forces at the shell surface or acoustic point-sources in the interior fluid. The time factor $\exp(-i\omega t)$ is omitted from all equations. The geometry is shown in Figure 1. The mathematics is presented with a minimum of elaboration and explanation because much of it has been given in greater detail elsewhere [2,3].

(b) Pressure and Particle Displacements Inside Pipe

The excitation is assumed to be of even ϕ-dependence so the pressure, radial displacement and axial displacement can be expressed as the Fourier transforms

$$\begin{vmatrix} p_1(r,\phi,z) \\ u_{r1}(r,\phi,z) \\ u_{z1}(r,\phi,z) \end{vmatrix} = (1/2\pi) \sum_{n=0}^{\infty} \cos(n\phi) \int_{-\infty}^{\infty} \exp(i\alpha z) \begin{vmatrix} \bar{p}_1(r,n,\alpha) \\ \bar{u}_{r1}(r,n,\alpha) \\ \bar{u}_{z1}(r,n,\alpha) \end{vmatrix} d\alpha \qquad (2.1)$$

The spectral pressure is of the form [2,3]

$$\bar{p}_1(r,n,\alpha) = \rho_1 w^2 [J_n(b_1 r)/b_1 J_n'(b_1 a)] \bar{W}(n,\alpha) + \bar{A}(r,n,\alpha) \qquad (2.2)$$

where $\bar{W}(n,\alpha)$ is the radial spectral displacement at the shell surface and $\bar{A}(r,n,\alpha)$ is identically zero for point-force excitation. A matrix formula for $\bar{W}(n,\alpha)$ for the special case of Goldenveizer-Novozhilov shell theory [8] is given in the Appendix. For point source excitation [2,3]

$$\bar{A}(r,n,\alpha) = \pi p_o e_n [J_n(b_1 x_o)/J_n'(b_1 a)][J_n(b_1 r)Y_n'(b_1 a) - Y_n(b_1 r)J_n'(b_1 a)], \quad r>x_o \qquad (2.3)$$

$$= \pi p_o e_n [J_n(b_1 r)/J_n'(b_1 a)][J_n(b_1 x_o)Y_n'(b_1 a) - Y_n(b_1 x_o)J_n'(b_1 a)], \quad r<x_o$$

The radial and axial acoustic particle displacements are related to the pressure by the formula

$$[\partial p_1/\partial r, \ \partial p_1/\partial z] = \rho_1 w^2 [u_{r1}, \ u_{z1}] \qquad (2.4)$$

from which the spectral displacements

$$\bar{u}_{r1}(r,n,\alpha) = [J_n'(b_1 r)/J_n'(b_1 a)] \bar{W}(n,\alpha) + (\rho_1 w^2)^{-1} \partial \bar{A}(r,n,\alpha)/\partial r \qquad (2.5)$$

$$\bar{u}_{z1}(r,n,\alpha) = i\alpha [J_n(b_1 r)/b_1 J_n'(b_1 a)] \bar{W}(n,\alpha) + i\alpha (\rho_1 w^2)^{-1} \bar{A}(r,n,\alpha) \qquad (2.6)$$

may be obtained by the use of equations (2.1-2.3). In equation (2.5)

$$\partial \bar{A}/\partial r = \pi p_o e_n [J_n(b_1 x_o)/J_n'(b_1 a)] b_1 [J_n'(b_1 r)Y_n'(b_1 a) - Y_n'(b_1 r)J_n'(b_1 a)], \quad r>x_o$$

$$= \pi p_o e_n [J_n'(b_1 r)/J_n'(b_1 a)] b_1 [J_n(b_1 x_o)Y_n'(b_1 a) - Y_n(b_1 x_o)J_n'(b_1 a)], \quad r<x_o \qquad (2.7)$$

(c) Exterior Pressure and Particle Displacements

The exterior pressure, radial and axial displacements have the Fourier transform representations

$$\begin{vmatrix} p_2(r,\phi,z) \\ u_{r2}(r,\phi,z) \\ u_{z2}(r,\phi,z) \end{vmatrix} = (1/2\pi) \sum_{n=0}^{\infty} \cos(n\phi) \int_{-\infty}^{\infty} \exp(i\alpha z) \begin{vmatrix} \bar{p}_2(r,n,\alpha) \\ \bar{u}_{r2}(r,n,\alpha) \\ \bar{u}_{z2}(r,n,\alpha) \end{vmatrix} d\alpha \tag{2.8}$$

The spectral pressure in the absence of exterior sound sources is

$$\bar{p}_2(r,n,\alpha) = \rho_2 w^2 [H_n(b_2 r)/b_2 H_n'(b_2 a)] \bar{W}(n,\alpha) \tag{2.9}$$

where $\bar{W}(n,\alpha)$ is the spectral displacement at the shell surface. The fluid particle displacements are simply

$$\begin{aligned} \bar{u}_{r2}(r,n,\alpha) &= [H_n'(b_2 r)/H_n'(b_2 a)] \bar{W}(n,\alpha) \\ \bar{u}_{z2}(r,n,\alpha) &= i\alpha [H_n(b_2 r)/b_2 H_n'(b_2 a)] \bar{W}(n,\alpha) \end{aligned} \tag{2.10}$$

(d) Intensity Vectors in (r,z) Plane

The radial and axial components of the time and ϕ-averaged interior intensity vector are defined as

$$\begin{aligned} I_r(r,z) &= \tfrac{1}{4} \sum_{n=0}^{\infty} p_{n1}^*(r,z) \dot{u}_{nr1}(r,z) \\ I_z(r,z) &= \tfrac{1}{4} \sum_{n=0}^{\infty} p_{n1}^*(r,z) \dot{u}_{nz1}(r,z) \end{aligned} \tag{2.11}$$

where

$$\begin{vmatrix} p_{n1}(r,z) \\ \dot{u}_{nr1}(r,z) \\ \dot{u}_{nz1}(r,z) \end{vmatrix} = (1/2\pi) \int_{-\infty}^{\infty} \exp(i\alpha z) \begin{vmatrix} \bar{p}_1(r,n,\alpha) \\ -iw\bar{u}_{r1}(r,n,\alpha) \\ -iw\bar{u}_{z1}(r,n,\alpha) \end{vmatrix} i\alpha \tag{2.12}$$

The amplitude and phase of the intensity vector are

$$I(r,z) = [I_r^2(r,z) + I_z^2(r,z)]^{\frac{1}{2}}, \quad \theta(r,z) = \tan^{-1}[I_r/I_z] \tag{2.13}$$

The acoustic intensity vector in the exterior fluid is defined in the same way, except that a subscript 2 replaces the subscript 1.

3. NUMERICAL EVALUATION OF INTEGRALS

The integrals in equations (2.12) must be evaluated numerically because closed-form expressions are not available. Their numerical approximation, on truncating the infinite limits to finite values, is based on a simple adaptive Gaussian quadrature scheme of order 2 that has been used [3] to evaluate similar integrals. Because the Fourier integral transform representation is arbitrary with respect to a solution of the homogeneous equations, it is necessary to introduce damping into the system before numerical evaluation is possible. The usual procedure is adopted here to include dissipation, viz set $E=E(1-i\eta_s)$ and $c=c(1-i\eta_f)$ where η_s and η_f are the hysteretic loss factors in the shell wall and fluid respectively,

When the excitation is a radial force or source located at z=0, then the computational times may be halved by writing equations (2.12) in the form

$$\begin{vmatrix} p_{nl}(r,z) \\ \dot{u}_{nrl}(r,z) \\ \dot{u}_{nzl}(r,z) \end{vmatrix} = (1/2\pi) \int_0^{\infty} \begin{vmatrix} 2\tilde{p}_l(r,n,\alpha)\cos(\alpha z) \\ -2iw\tilde{u}_{rl}(r,n,\alpha)\cos(\alpha z) \\ 2w\tilde{u}_{zl}(r,n,\alpha)\sin(\alpha z) \end{vmatrix} d\alpha \qquad (3.1)$$

It is also evident that further savings in computer time are possible by parallel computation at an array of z-values, due to the simplicity of the z-dependent term in relation to the r-dependent term. Methods based on the fast Fourier transform algorithm are unlikely to be of much greater efficiency.

4. NUMERICAL EXAMPLES

(a) General

For the particular case of a water-filled shell surrounded by a vacuum, Figures 2-3 show wave-number-frequency plots and Figures 4-10 show intensity vector plots for the n=0 and 2 harmonics separately. The material and geometric constants in SI units that have been used in the computations are as follows:

steel: $E=19.5\times10^{10}$ $\sigma=0.29$ $\rho=7700.0$ $h=0.01$ $a=0.10$ $\eta_s=0.02$

water: $\rho=1000.0$ $c=1500.0$ $\eta_f=0.001$

The radial point-force was located at the cylindrical coordinates (a,0,0) and the interior point-source was located at the point (2a/3,0,0). The fluid loss-factor, $\eta_f=0.001$, is sufficiently large enough to allow numerical integration of equations (3.1) without ill-conditioning, yet it is sufficiently small to avoid significant attenuation in the fluid over the maximum axial distance considered, viz 0.4m.

The intensity vector plots are shown for the separate values of the circumferential harmonic, n, in order to aid interpretation via the wave-number versus frequency plots; also, the individual intensities have

physical meaning because they are measureable. Due to the symmetry of the excitations, the intensity vectors are plotted for $z>0$ only; plots for $z<0$ are simply mirror images. In all Figures the plotted lengths of the normalised vectors are proportional to $\sqrt{I(r,z)}$.

(b) Wavenumber-Frequency Plots

The wavenumbers for free-wave propagation in the axial direction are those real values of α for which the determinant of the matrix equation (A1) vanishes. Plots of these values versus frequency, for a selected value of n, are called axial wavenumber versus frequency plots. The physical interpretation of these plots is described elsewhere [1]; in particular, the changing nature of each branch with frequency is of central importance as its energy ratios between shell and fluid may alter considerably.

Figure 2 contains the wavenumber-frequency plots of a steel pipe whose interior and exterior are vacuums. Superimposed on these plots are the wavenumbers of a rigid-walled circular duct of water. Figure 3 contains the plots for a steel pipe containing water: briefly, for n=0 the branches labelled 1-4 cut-on close to a plane fluid wave, an axial shell wave, a radial shell wave and a fluid wave, respectively - the branch '0' is a wave of pure torsion; for n=2 the branches labelled 1-3 cut-on close to a radial shell wave, a fluid wave and a torsional wave, respectively.

(c) Rigid Shell: Source Excitation

Figures 4a and 4b show the intensity vectors of the n=0 harmonic at frequencies of 4 and 12kHz, respectively. The plane wave mode alone propagates at 4kHz, while at 12kHz it is just evident that the two propagating modes are combining to form a 'weak' interference pattern. The intensity vectors on the shell axis must be parallel to that axis because the fluid particle velocity in the radial direction vanishes there.

Figures 5a and 5b show the intensity vectors of the n=2 harmonic at frequencies of 4 and 12kHz, respectively. At 4kHz the intensity vectors decay rapidly with distance because of the absence of a propagating mode, while at 12kHz there is a single propagating mode. The intensity vectors on the shell axis must vanish because both pressure and particle velocities are identically zero there.

(d) Steel Shell: Source Excitation

Figures 6 and 7 show the intensity vectors of the n=0 harmonic at the frequencies of 7.25 and 12kHz, respectively. A plot at 4kHz is not shown because it has much the same appearance as the plot of Figure 4a, except that the vectors at the shell centre have marginally smaller magnitudes. At 7.25kHz, which is just above the cut-on frequency of the radial shell mode, modal interference effects and areas of energy circulation are clearly evident; also, there is an interchange of energy

between the fluid and the shell. Similar remarks apply to the plot at 12kHz. Schultz[9] notes that areas of acoustic energy circulation are the rule rather than the exception in acoustic fields; they are even present in standing-wave fields due to the superposition of modes whose individual intensities vanish!

Figure 8 shows the intensity vectors for the n=2 harmonic at 4kHz where there is a single propagating mode. Most of the energy from the source immediately enters the shell, and the propagating fluid surface wave associated with a radial shell wave is evident. At 12kHz, not shown here, the n=2 plot is little different from the rigid shell plot of Figure 5b.

(e) Steel Shell: Force Excitation

Figure 9 is the plot of the n=0 harmonic at 7.25kHz. It has many features in common with Figure 6 (the plot with source excitation) with the interchange of energy between fluid and shell being particularly marked. Figure 10 is the vector plot of the n=2 harmonic at 12kHz. In the range $r<a/2$, a comparison with Figure 5b shows that the energy is due to an essentially fluid-type mode; however, in the range $r>a/2$, interference between shell and fluid modes results in a considerable interchange of energy between fluid and shell.

5. CONCLUDING REMARKS

Formulae have been given from which the acoustic intensity vectors interior and exterior to an elastic shell may be calculated numerically. Enthusiasts of wave propagation problems will find the work of Fuller and Fahy [1] a valuable aid to their interpretation. The limited number of plots of interior vectors, due to point-force or point-source excitation, that are presented are of sufficient interest to justify further numerical work to enhance their physical interpretation and their practical usefulness in noise control.

First, it is necessary to obtain intensity vector plots for an extended range of parameters that include:

(i) sufficiently small frequency steps;
(ii) the individual (n=0,1,2) harmonics together with their sum;
(iii) the presence of an exterior fluid;
(iv) a range of shell materials.

This extended range of plots together with wavenumber versus frequency plots should assist the understanding of wave propagation in and sound radiation from fluid-filled pipes.

Secondly, intensity vectors in the presence of point or axisymmetric constraints on the shell surface may be of practical value to investigations into wave transmission phenomena in complex piping networks in

which non-uniformities are common. No new procedure is involved here; the method of dynamic stiffness coupling can be used to determine the reaction forces caused by the constraints, whence the determination of the intensity vectors proceeds in an uncomplicated way. The procedure to be followed is given in Spicer's report [7].

6. ACKNOWLEDGEMENT

Thanks are due to E.J. Clement for his help with the graphical presentations.

J.H. James (PSO)

REFERENCES

1. FULLER, C.R., FAHY F.J., Characteristics of wave propagation and energy distribution in cylindrical elastic shells filled with fluid, J. Sound Vib., 81(4), 1982, pages 501-518.

2. JAMES, J.H., Sound radiation from fluid-filled pipes, Admiralty Marine Technology Establishment, Teddington, AMTE(N)TM81048, September 1981.

3. JAMES, J.H., Computation of acoustic power, vibration response and acoustic pressures of fluid-filled pipes, Admiralty Marine Technology Establisment, Teddington, AMTE(N)TM82036, May 1982.

4. FAHY, F.J., A technique for measuring sound intensity with a sound level meter, Noise Control Engineering, 9(3), 1977, pages 155-162.

5. FAHY, F.J., Measurements with an intensity meter of the acoustic power of a small machine in a room, J. Sound Vib., 57(3), 1978, pages 311-322.

6. REINHART, T.E., CROCKER, M.J., Source identification on a diesel engine using acoustic intensity measurements, Noise Control Engineering, 18(3), 1982, pages 84-92.

7. SPICER, W.J., Acoustic intensity vectors from an infinite plate with line attachments, Admiralty Marine Technology Establishment, Teddington, AMTE(N)TM81086, October 1981.

8. LEISSA, A.W., Vibration of shells, NASA SP-288, 1973.

9. SCHULTZ, T.J., et al, Measurement of acoustic intensity in reactive sound field, J. Acoust. Soc. Am., 57(6) Part 1, 1975, pages 1263-1268.

APPENDIX

The Spectral Displacements

The excitation is either a radial point force, of magnitude F_o, that is located at the cylindrical coordinates $(a,0,0)$, or it is an interior point source of sound, of free-field pressure $p_o \exp(ik_1 R_o)/R_o$, that is located at $(x_o,0,0)$. The spectral displacements are obtained, via Novozhilov shell theory [8], as the solution of the matrix equation that relates displacements to external excitations [2]

$$\begin{vmatrix} S_{11} & S_{12} & S_{13} \\ S_{21} & S_{22} & S_{23} \\ S_{31} & S_{32} & S_{33} + \rho_2 w^2 H_n(b_2 a)/b_2 H_n'(b_2 a) \\ & & - \rho_1 w^2 J_n(b_1 a)/b_1 J_n'(b_1 a) \end{vmatrix} \begin{vmatrix} \overline{U}(n,\alpha) \\ \overline{V}(n,\alpha) \\ \overline{W}(n,\alpha) \end{vmatrix} = \begin{vmatrix} 0 \\ 0 \\ F_o e_n / 2\pi a \text{ or} \\ 2 p_o e_n J_n(b_1 x_o)/b_1 a J_n'(b_1 a) \end{vmatrix} \tag{A1}$$

where

$$\begin{aligned} S_{11} &= E_1[\alpha^2 + n^2(1-\sigma)/2a^2] - \rho_s h w^2 \\ S_{12} &= -E_1 i\alpha n(1+\sigma)/2a \\ S_{13} &= -E_1 i\alpha\sigma/a \\ S_{21} &= -S_{12} \\ S_{22} &= E_1[\alpha^2(1-\sigma)/2 + n^2/a^2 + 2\alpha^2\beta^2(1-\sigma) + \beta^2 n^2/a^2] - \rho_s h w^2 \\ S_{23} &= E_1[n/a^2 + n\alpha^2\beta^2(2-\sigma) + n^3\beta^2/a^2] \\ S_{31} &= -S_{13} \\ S_{32} &= S_{23} \\ S_{33} &= E_1[1/a^2 + \alpha^4\beta^2 a^2 + 2n^2\alpha^2\beta^2 + n^4\beta^2/a^2] - \rho_s w^2 h \end{aligned} \tag{A2}$$

An axial point force excitation is obtained by setting the right-hand side of the matrix equation to $[F_o e_n/2\pi a, 0, 0]^T$.

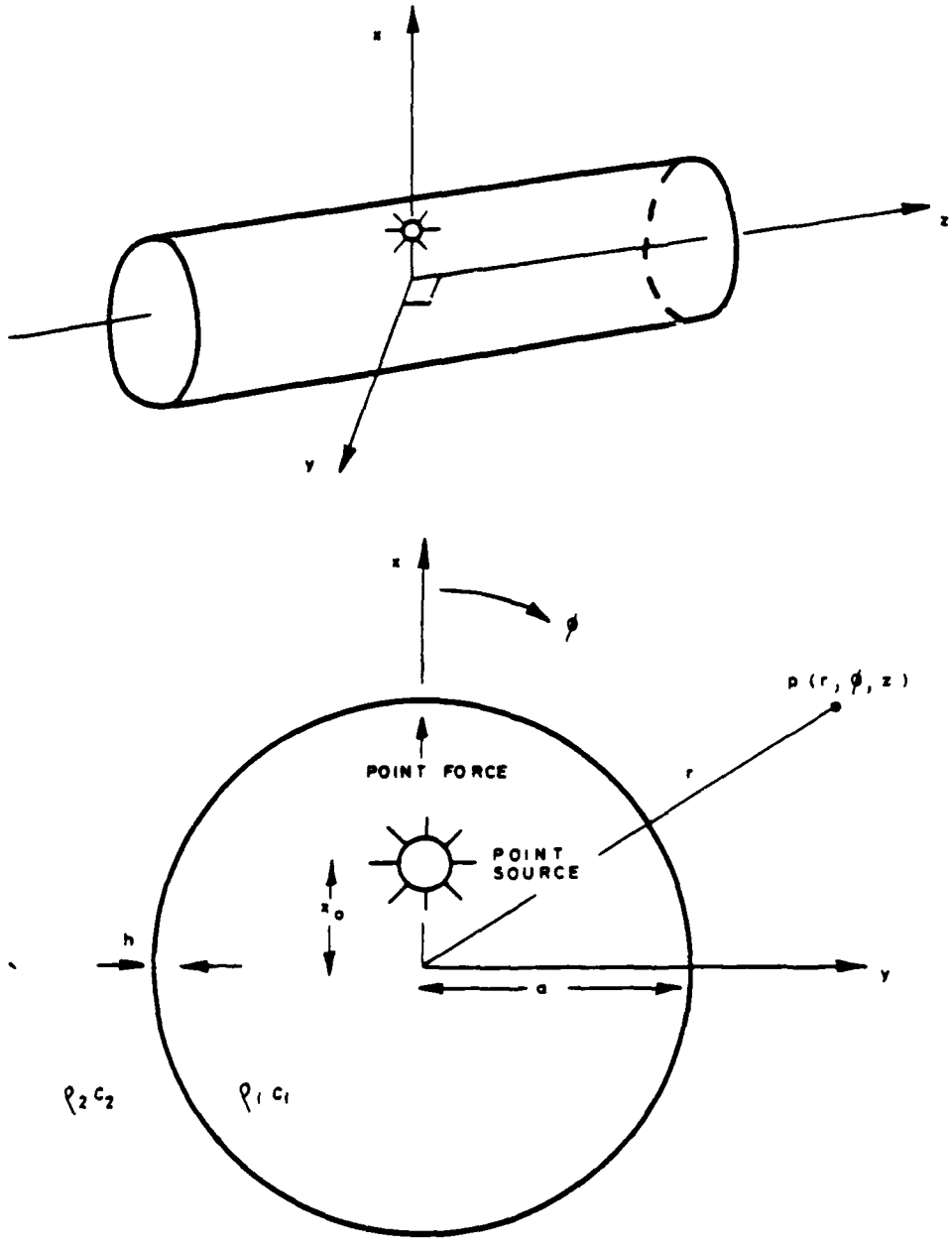

$$x = r.\cos(\phi)$$

$$y = r.\sin(\phi)$$

$$z = z$$

FIG.1 GEOMETRY AND COORDINATE SYSTEMS

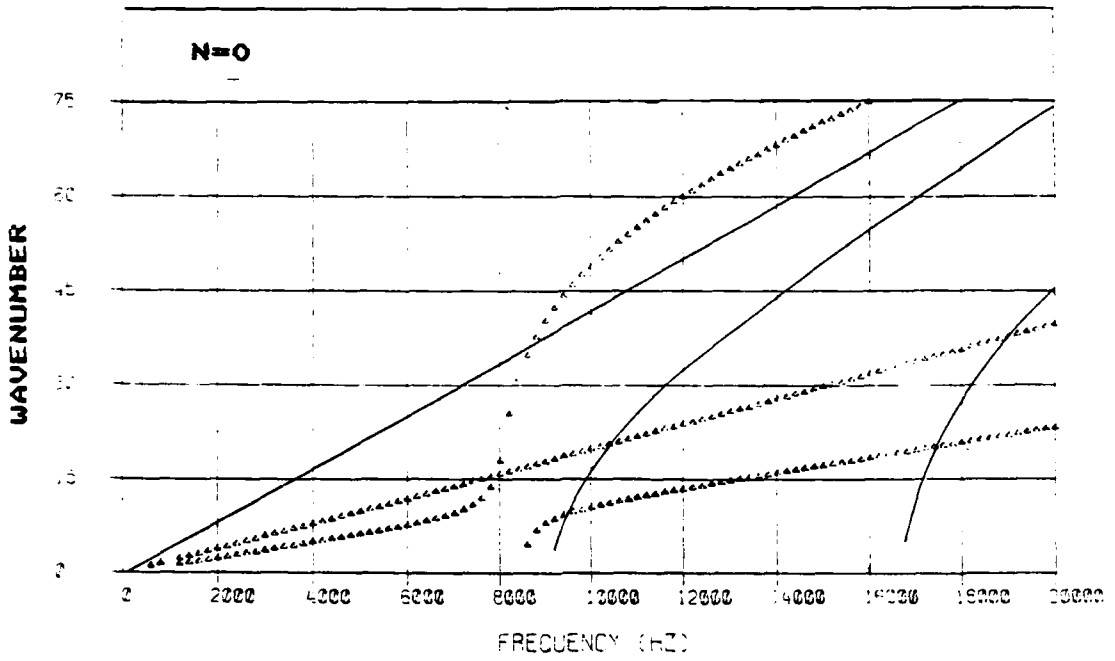

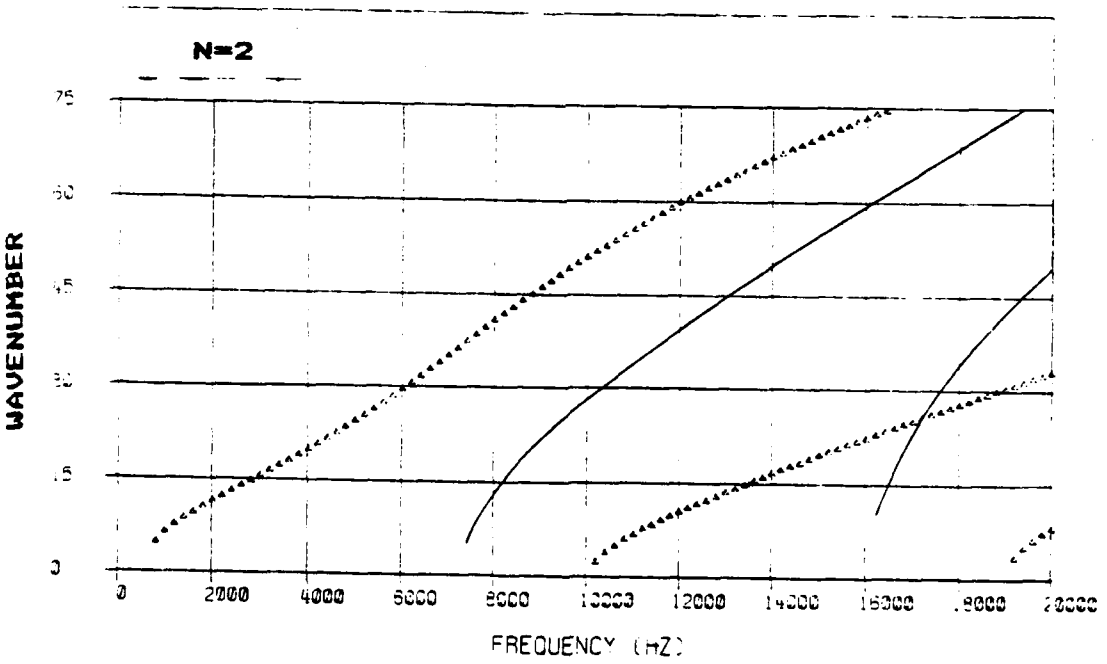

FIG.2 AXIAL WAVENUMBER VERSUS FREQUENCY.
SHELL IN VACUO ΔΔΔΔ
RIGID-WALLED DUCT OF WATER ——

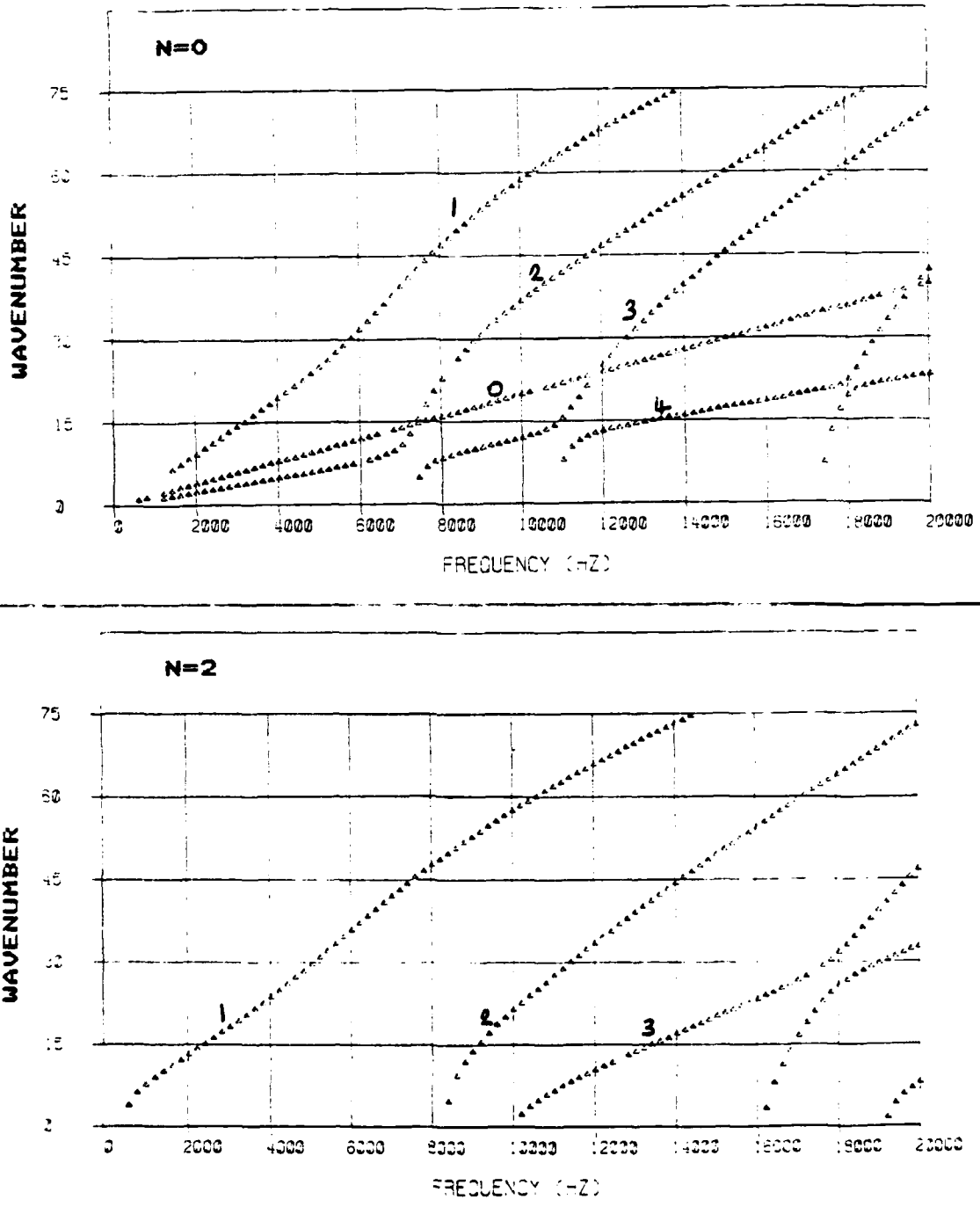

FIG.3 AXIAL WAVENUMBER VERSUS FREQUENCY. SHELL WITH INTERIOR WATER EXTERIOR VACUUM.

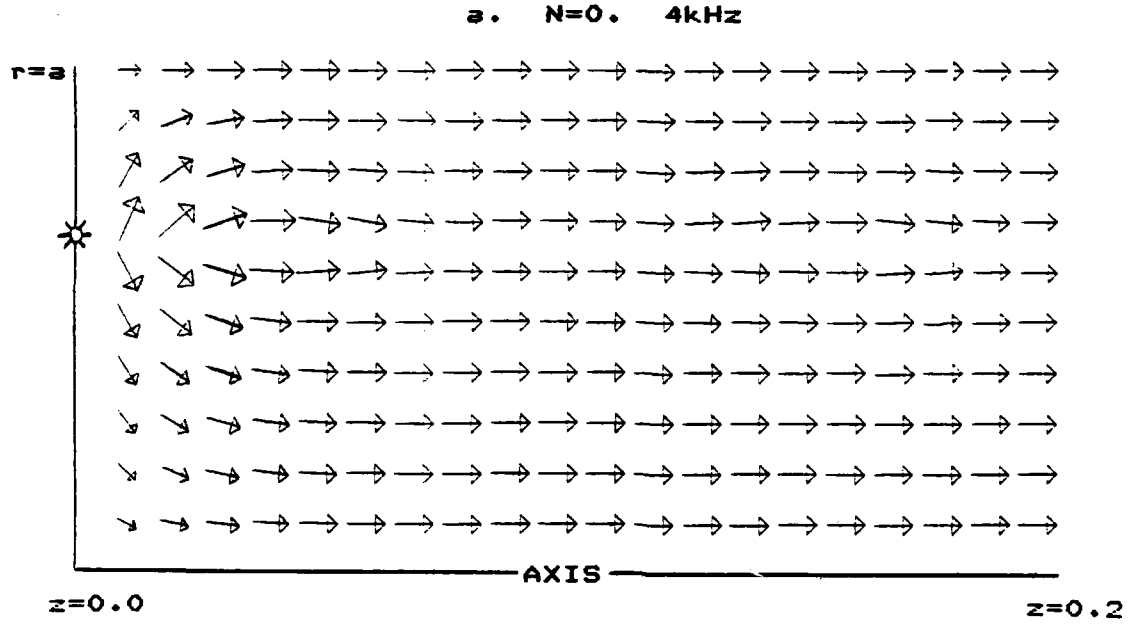

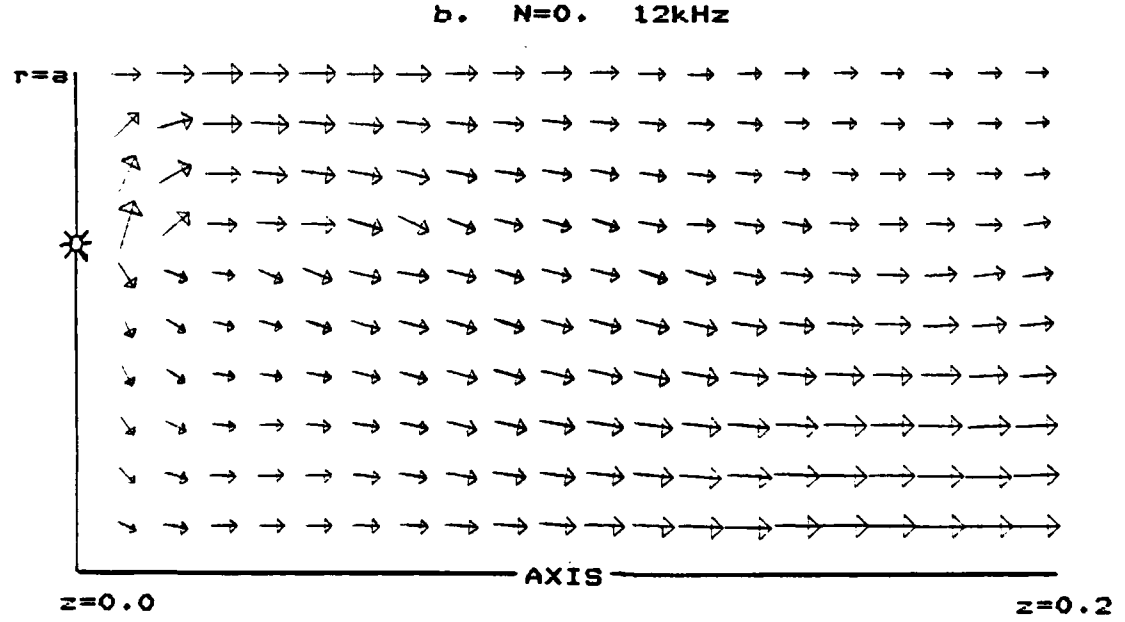

FIG. 4 POINT SOURCE EXCITATION. RIGID SHELL. N=0.

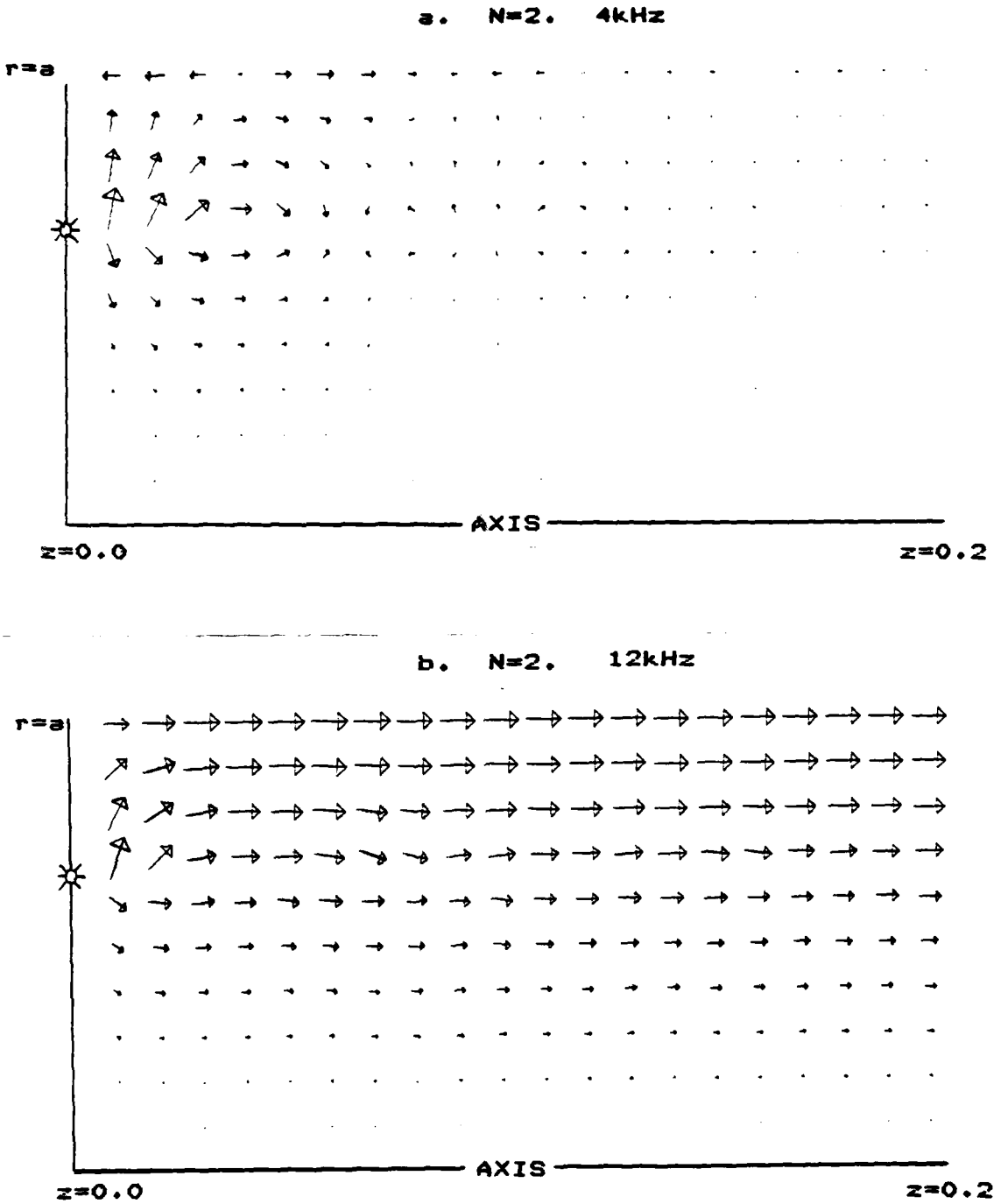

FIG. 5 POINT SOURCE EXCITATION. RIGID SHELL. N=2.

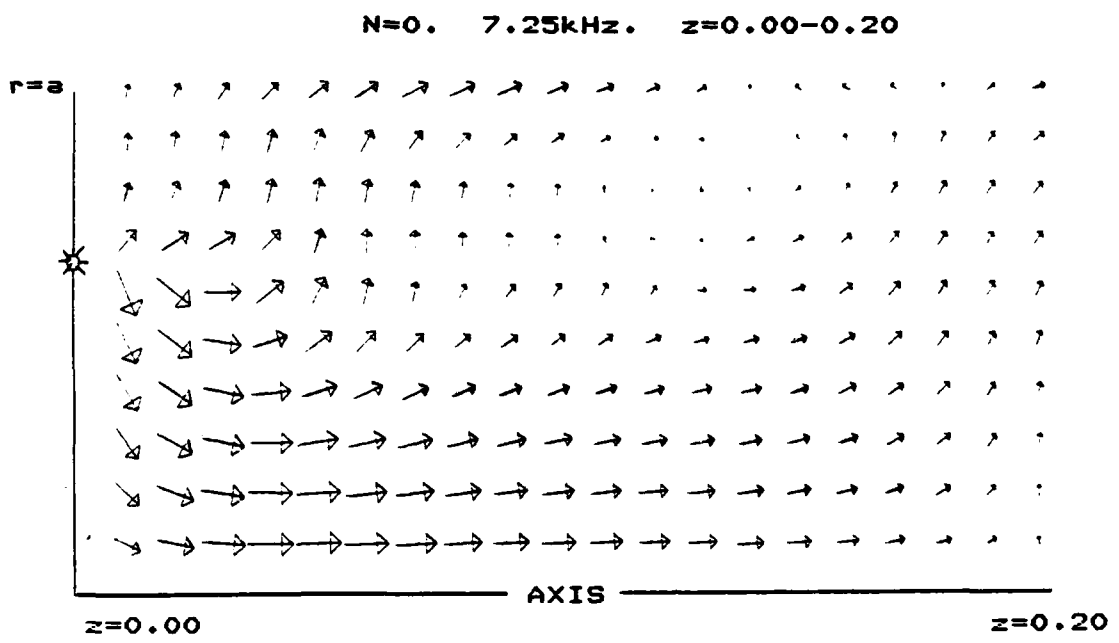

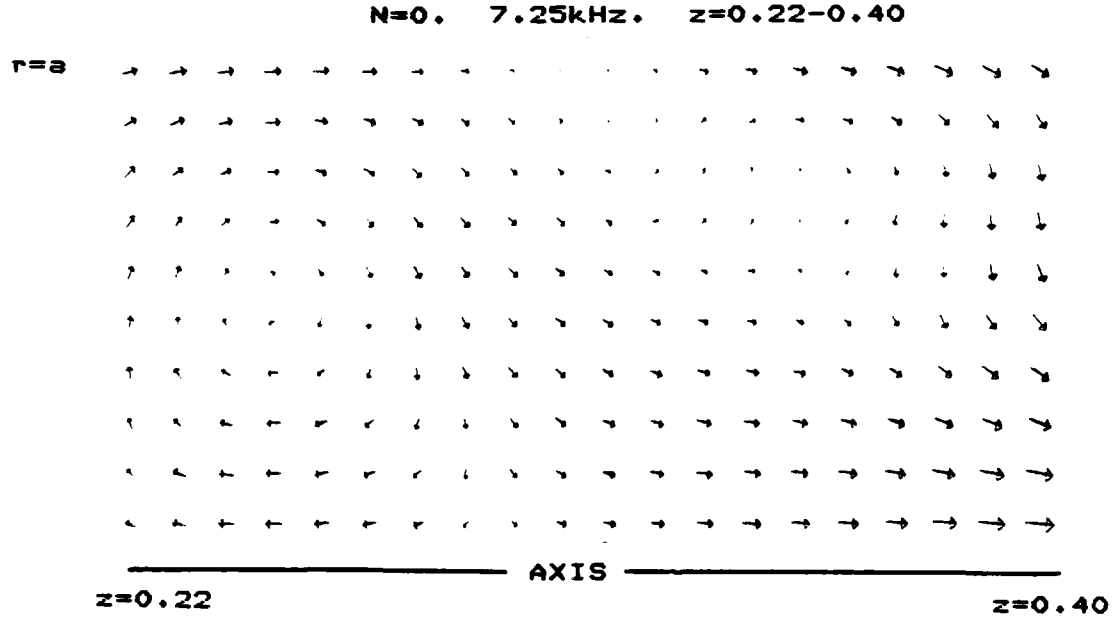

FIG. 6 POINT SOURCE EXCITATION. STEEL SHELL. N=0.

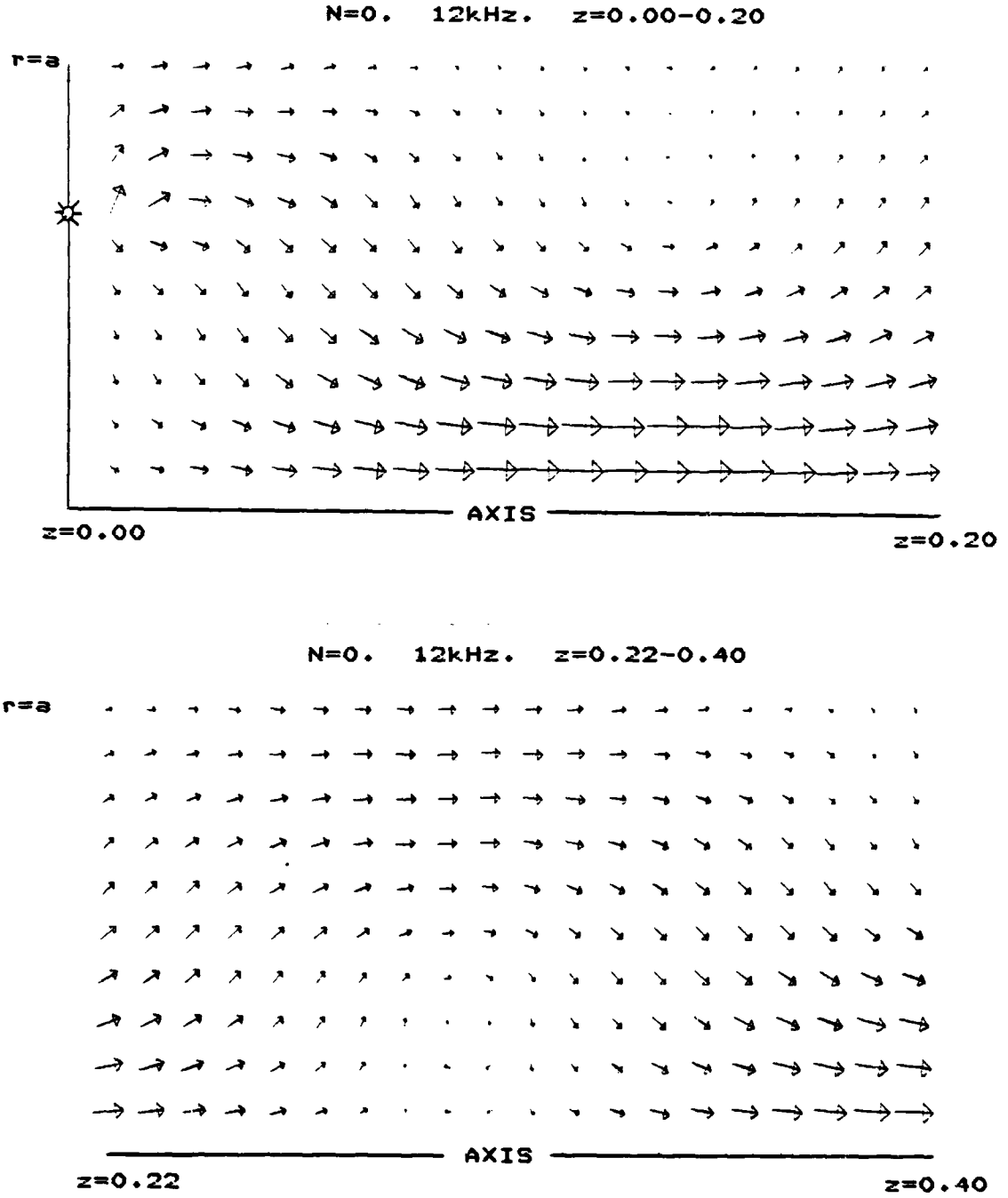

FIG. 7 POINT SOURCE EXCITATION. STEEL SHELL. N=0.

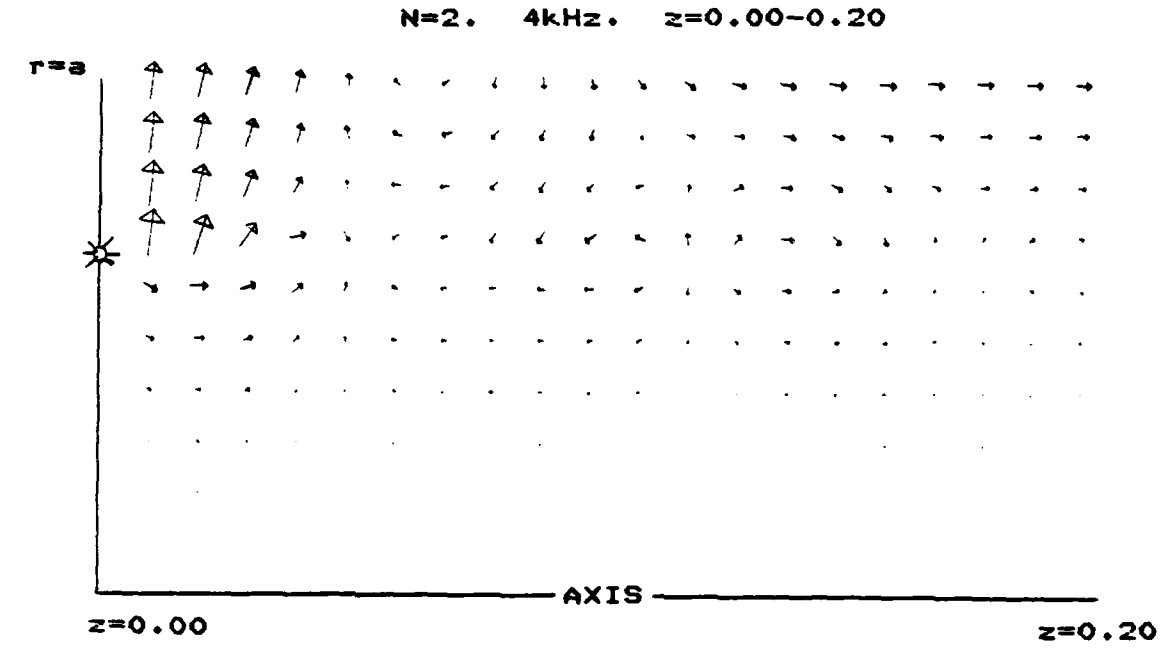

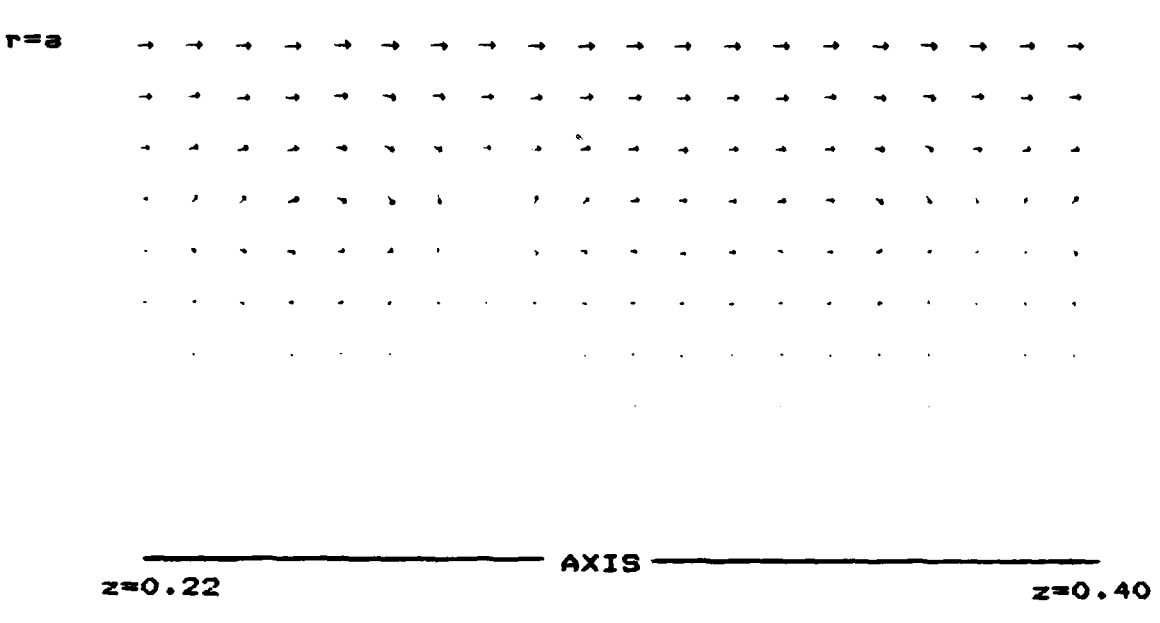

FIG. 8 POINT SOURCE EXCITATION. STEEL SHELL. N=2.

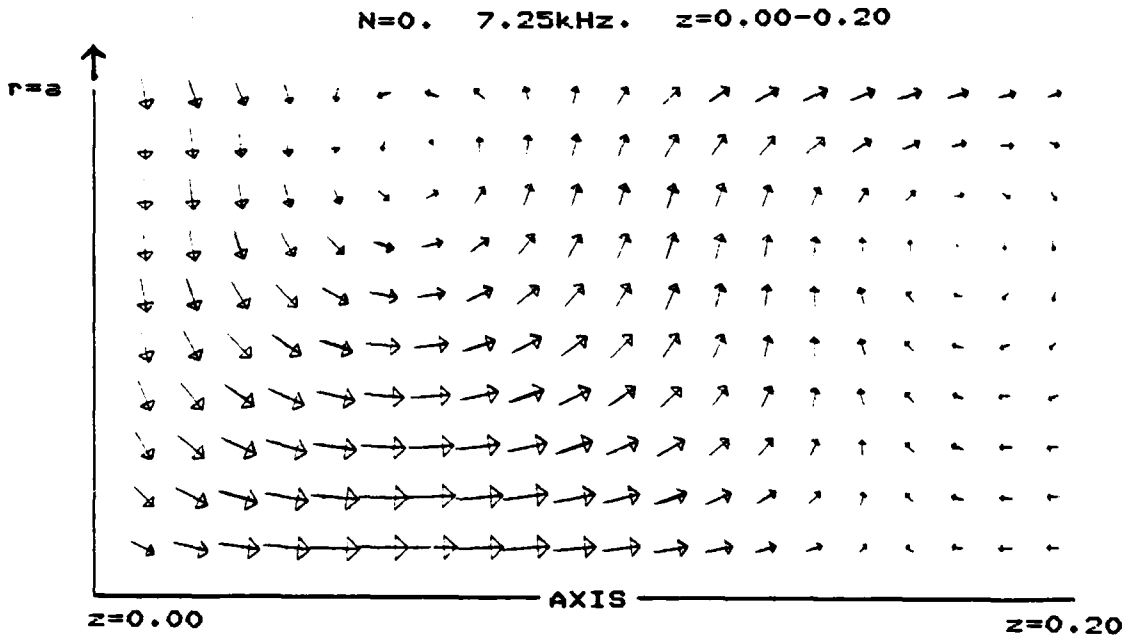

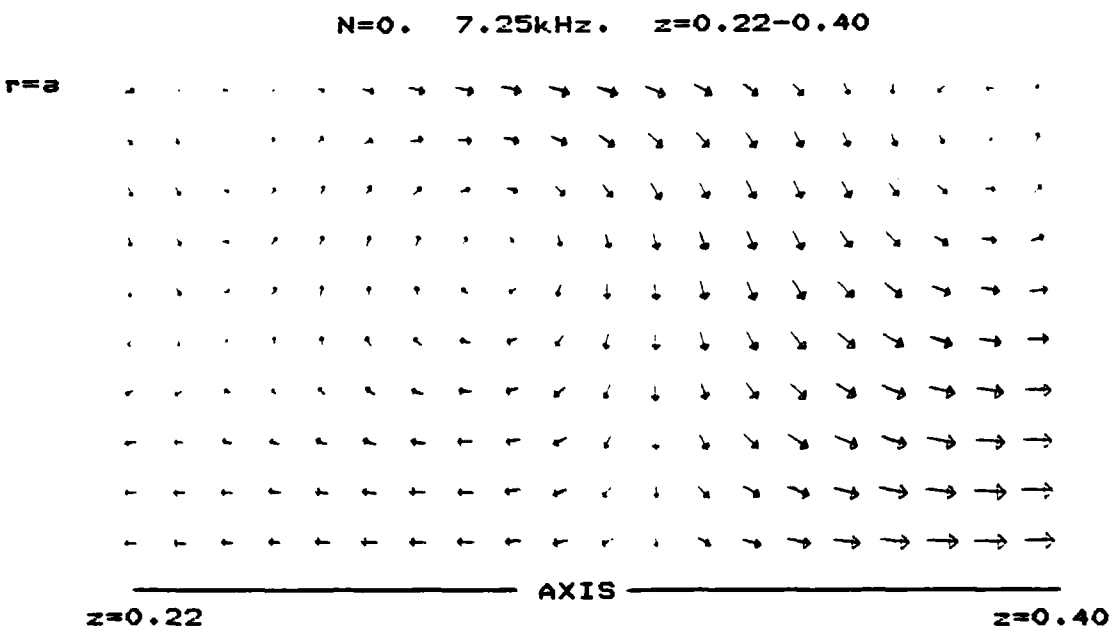

FIG. 9 POINT FORCE EXCITATION. STEEL SHELL. N=0.

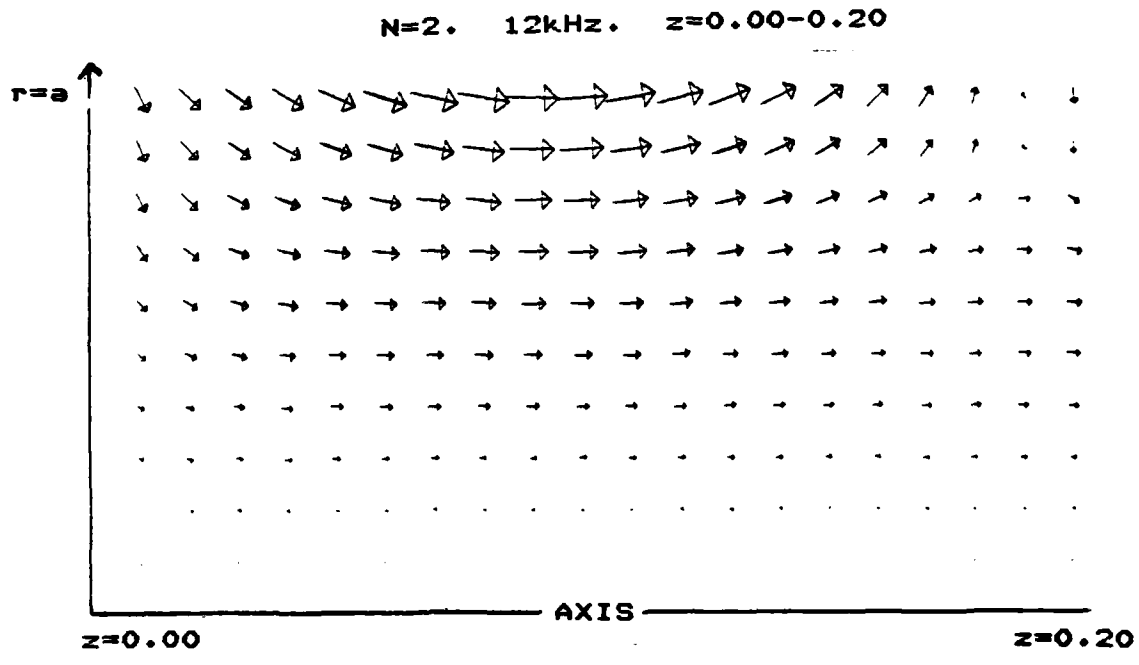

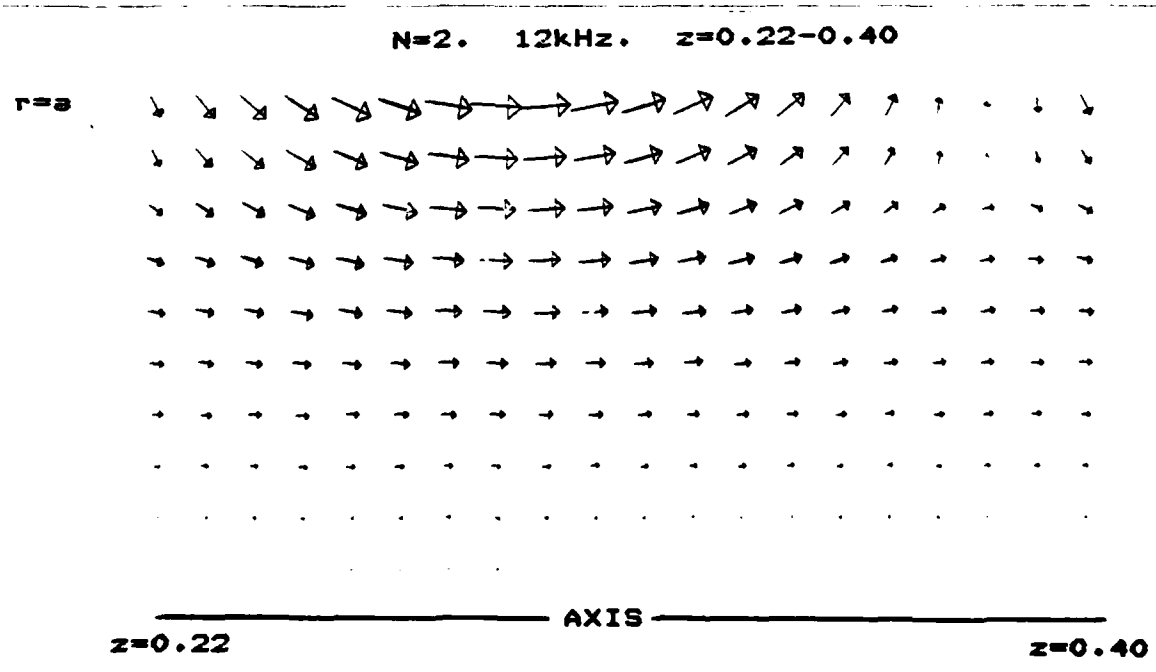

FIG. 10 POINT FORCE EXCITATION. STEEL SHELL. N=2.

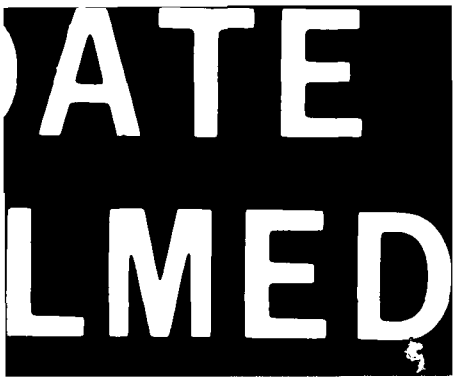
ATE
LMED